BCSJ

# Syntheses and Redox Properties of Complexes with $Mo_3S_4$ Cores and Tridentate Schiff Base Ligands

**Keisuke Kawamoto,*[1] Akio Ichimura,[1] Hideki Hashimoto,[2,3] Isamu Kinoshita,[1,3] and Takanori Nishioka*[1]**

[1]Department of Chemistry, Graduate School of Science, Osaka City University, 3-3-138 Sugimoto, Sumiyoshi-ku, Osaka 558-8585

[2]Department of Physics, Graduate School of Science, Osaka City University, 3-3-138 Sugimoto, Sumiyoshi-ku, Osaka 558-8585

[3]The OCU Advanced Research Institute for Natural Science and Technology (OCARINA), Osaka City University, 3-3-138 Sugimoto, Sumiyoshi-ku, Osaka 558-8585

E-mail: nishioka@sci.osaka-cu.ac.jp
Received: September 12, 2014; Accepted: November 3, 2014; Web Released: November 10, 2014

A series of potentially tridentate Schiff base ligands, {HOPhC=N-$(CH_2)_3$-XMe: X = S (HLSMe), Se (HLSeMe)}, was prepared by condensation reactions of salicylaldehyde and the corresponding functionalized propylamines. These ligands were used to form the monocationic complexes, $[Mo_3S_4(LXMe)_3]^+$ (X = S (**1**$^+$), Se (**2**$^+$)), through treatment of $[Mo_3S_4(H_2O)_9]^{4+}$ with the appropriate Schiff base ligand in methanol. Single-crystal X-ray structural analysis of **1-PF$_6$** revealed that one Schiff base ligand coordinates to each Mo via the O, N, and SMe donor atoms, and then the mono cationic cluster $[Mo_3S_4(LSMe)_3]^+$ has a pseudo $C_3$ symmetry if the chirality around the coordinated sulfur atoms is not taken into account. Because of the arrangements of the asymmetric Schiff base ligand, this monocationic cluster possibly adopts one of two axial chiralities. Furthermore, each sulfur atom of the three coordinated SMe groups in the complex cation is also chiral affording the two enantiomers observed in the unit cell. Dynamic behaviors of complexes **1-PF$_6$** and **2-PF$_6$** in solution were examined using line shape analyses of variable temperature NMR spectra revealing that the rate constant of the chiral inversion at the S atoms in **1-PF$_6$** is greater than that at the Se atoms in **2-PF$_6$** and the difference in the $\Delta H^{\ddagger}$ values of **1-PF$_6$** (47.1 kJ mol$^{-1}$) and **2-PF$_6$** (56.7 kJ mol$^{-1}$) and the negative $\Delta S^{\ddagger}$ values (−39.9 and −57.5 J mol$^{-1}$ K$^{-1}$ for **1-PF$_6$** and **2-PF$_6$**, respectively) suggest that the inversion processes involve bond cleavage between the metal centers and S or Se atoms followed by coordination of solvent molecules. The electrochemical properties of **1-PF$_6$** and **2-PF$_6$** were evaluated using cyclic voltammetry and this revealed that both **1**$^+$ and **2**$^+$ exhibit two consecutive, reversible one-electron reduction waves that are assigned to formal Mo(IV IV IV)/Mo(III IV IV) and Mo(III IV IV)/Mo(III III IV) couples, respectively. The ability of **1-PF$_6$** and **2-PF$_6$** to catalyze the electroreduction of $H^+$ was also examined using $CH_3CO_2H$ or $CF_3CO_2H$ as a proton source. Noteworthy, the redox potentials for the catalytic wave depend on the acidity of the added acids. Thus, the catalytic current around the first reduction wave is observed in the presence of the stronger trifluoroacetic acid as a proton source, while the current around the second reduction wave appears when the weaker acetic acid is used.

Currently, very large amounts of hydrogen are produced and consumed on a daily basis by industry for a range of important processes including the production of $NH_3$. However, this hydrogen is almost invariably produced by using fossil fuels as a raw material and source of energy.[1] The development of efficient and sustainable methods for the production of hydrogen that do not utilize fossil fuels is an area of research that is under intensive investigation.[2] It has been demonstrated that platinum particles or complexes can catalyze the electrochemical reduction of protons affording hydrogen.[3] In nature, enzymes such as hydrogenase and nitrogenase catalyze the reduction of protons and nitrogen, respectively, and many coordination compounds that mimic the active centers of these enzymes have been synthesized and investigated to develop efficient catalysts for hydrogen production using nonprecious metals. Molybdenum–sulfur units are essential components of the active center of one of the nitrogenases, and nanoparticles of $MoS_2$ have attracted much attention as excellent hydrogen evolution reaction (HER) catalysts.[4]

Molybdenum can adopt a wide range of oxidation states (from 0 to +6) and its complexes exhibit a variety of reactivity. One class of molybdenum complexes that show intriguing chemistry are those based on the incomplete cuboidal clusters ($Mo_3X_4$: X = O, S, or Se) in which the oxygen, sulfur, or selenium ligands, bridge the molybdenum(IV) ions.[5,6] Among these complexes, those based on the $Mo_3S_4$ cluster core become more stable when the molybdenum ions are reduced from IV to III, as might be expected by consideration of the HSAB principle. Importantly, Shibahara et al. showed that the $Mo_3S_4$ cluster complex $[Mo_3S_4(Hnta)_3]^{2-}$ catalyzes the reduction of protons to afford hydrogen.[7] Also, Chorkendorff et al. reported that a $Mo_3S_4$ complex, $[Mo_3S_4(\eta^5\text{-Cp}')_3]^+$ (Cp′: methylcyclo-

pentadienyl), adsorbed on a p-type silicon semiconductor worked as a heterogeneous catalyst leading to quantitative hydrogen evolution on irradiation by visible light[8] and Hong et al. showed that a composite material of $[Mo_3S_4(H_2O)_9]^{4+}$ and $NaTaO_3$ catalyzes proton reduction and hydrogen evolution during water oxidation at the valence band edge of $NaTaO_3$.[9] While there have been many electrochemical studies of the redox and electrocatalytic properties of numerous hydrogenase model compounds in organic solvents such as acetonitrile,[10] there have been only a few reports of the catalytic reduction of protons by complexes containing the $Mo_3S_4$ core in organic media.

In this study, we describe the synthesis of the new complexes $[Mo_3S_4(LXMe)_3]^+$ (X = S or Se, **1**$^+$ or **2**$^+$; LXMe = Schiff base ligand) that contain the $Mo_3S_4$ core (Charts 1 and 2). The Schiff base ligands coordinated to the $Mo_3S_4$ core of these complexes were used not only to increase solubility in organic solvents but also to enhance the tuning properties of the complexes by the chemical modification of the substituents of the salicylaldimine moiety and the S or Se donating atoms. Coordination of these Schiff base ligands to the Mo center is stabilized by the chelate effect due to a bidentate coordination mode of the salicylaldimine moiety, and the S or Se donating atoms connected to the salicylaldimine moiety with flexible chains also help the formation of a stable coordination environment and, in addition, provide a vacant site on the metal center by dissociation from the metal center. We report details of the structures and redox properties of **1-PF$_6$** and **2-PF$_6$**.

## Experimental

**General Procedures and Materials.** 3-(Methylthio)-propylamine, salicylaldehyde, and 3-chloropropylamine hydrochloride were purchased from Tokyo Chemical Industry Co., Ltd. Ammonium hexafluorophosphate was purchased from Wako Pure chemicals. Sodium borohydride and potassium *tert*-butoxide were purchased from Nacalai Tesque. Dimethyl diselenide was purchased from Aldrich. All chemicals were used as received. NMR spectra were recorded on a LAMBDA 300 FT-NMR spectrometer. Chemical shifts are expressed in ppm downfield from $SiMe_4$ and are referenced to the proteo-impurity peaks in the deuterated solvents. Elemental analyses were performed by the Analytical Research Service Center at Osaka City University on a J-SCIENCE LAB JM10. FAB+ mass spectra were measured on a JMS-700T mass spectrometer using 3-nitrobenzylalcohol (NBA) as a supporting matrix. Electrochemical measurements were performed with an ALS/Chi model 680 electrochemical analyzer. The working and counter electrodes were a glassy carbon and a Pt wire, respectively. The reference electrode was a $Ag/Ag^+$ electrode. All the potential values were corrected referenced to the $Fc/Fc^+$ couple. Cyclic voltammograms were recorded at a scan rate of 100 mV s$^{-1}$ at room temperature using tetra-*n*-butylammonium hexafluorophosphate as a supporting electrolyte. Ligand preparations were performed under a $N_2$ atmosphere using Schlenk techniques.

**Synthesis of HLSMe (Scheme 1).** To a solution of salicylaldehyde (520 mg, 4.26 mmol) in deaerated methanol (10 mL), 3-(methylthio)propylamine (477 mg, 4.25 mmol) was added. The mixture was refluxed for 6 h. After the mixture was allowed to cool to room temperature, the solvent was removed under reduced pressure. The residue was dissolved in chloroform and the solution was washed with water (3 × 10 mL). The separated organic layer was dried with sodium sulfate. The solvent was removed on a rotary evaporator to afford HLSMe as an orange oily material in 81% yield (743 mg). $^1$H NMR ($CD_3CN$): $\delta$ 13.51 (s, br, 1H, Ph-O*H*), 8.48 (s, 1H, azomethine-*H*), 7.4–7.3 (m, 2H, Ph-*H*), 6.92 (t, 1H, $J$ = 8.1 Hz, Ph-*H*), 3.70 (t, 2H, $J$ = 7.3 Hz, C$H_2$), 2.59 (t, 2H, $J$ = 7.2 Hz, C$H_2$), 2.10 (s, 3H, SC$H_3$), 2.0 (m, 2H, C$H_2$).

**Synthesis of HLSeMe (Scheme 1).** To a solution of dimethyl diselenide (1.0 mL, 10.6 mmol) in ethanol (5 mL), a suspension of sodium borohydride (0.52 g, 13.8 mmol) in ethanol (5 mL) was added. After the mixture was stirred for 1 h at room temperature, a suspension of potassium *tert*-butoxide (1.45 g, 13.0 mmol) and 3-chloropropylamine hydrochloride (1.32 g, 10.2 mmol) in ethanol (40 mL) was added. The mixture was refluxed for 3 hours, and then a solution of salicylaldehyde (1.24 g, 10.1 mmol) in ethanol (10 mL) was added, and the mixture was refluxed for an additional 12 h. The mixture was cooled to room temperature and the organic phase was washed with water (3 × 10 mL). The separated organic layer was dried with sodium sulfate and then the solvent was removed on a rotary evaporator to give HLSeMe as an orange oily material in 92% yield (2.5 g). $^1$H NMR ($CD_3CN$): $\delta$ 13.47 (s, br, 0.8 H, Ph-O*H*), 8.45 (s, 1H, azomethine-*H*), 7.4–7.3 (m, 2H, Ph-*H*), 6.70 (t, 2H, $J$ = 7.5 Hz, Ph-*H*), 3.67 (t, 2H, $J$ = 6.7 Hz, C$H_2$), 2.60 (t, 2H, $J$ = 7.3 Hz, C$H_2$), 2.02 (t, 2H, $J$ = 7.10 Hz, C$H_2$), 1.97 (s, 3H, SeC$H_3$). $^{77}$Se NMR ($CD_3CN$): $\delta$ 183.13.

**Synthesis of $[Mo_3S_4(LSMe)_3]PF_6 \cdot 2CH_3CN$ (1-PF$_6$·2CH$_3$CN).** A sample of solid material containing the cation $[Mo_3S_4(H_2O)_9]^{4+}$ (0.12 mmol), which was obtained by removal of the solvent from a 5.61 mM solution of $[Mo_3S_4(H_2O)_9]^{4+}$

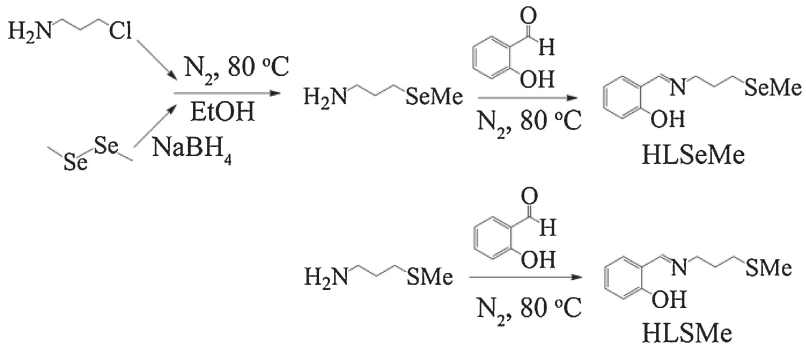


**Scheme 1.** Synthesis of HLSeMe and HLSMe.


 

(21.0 mL) in hydrochloric acid (concentration of the solution was determined using absorption spectrum, $\lambda_{max} = 620$ nm, $\varepsilon = 315\ M^{-1}\ cm^{-1}$),[7] was suspended in methanol (2 mL). A solution of HLSMe (78 mg, 0.37 mmol) in methanol (10 mL) was added to the suspension, and the mixture was stirred for 20 h at room temperature. After the solvent was removed under reduced pressure, the residue was dissolved in 2 mL of acetonitrile. After the insoluble solid was removed by filtration, $NH_4PF_6$ (20 mg, 0.12 mmol) was added to the filtrate. Diethyl ether was then carefully layered on top of this solution and the mixture was allowed to stand to give dark green crystals of $[Mo_3S_4(LSMe)_3]PF_6 \cdot 2CH_3CN$ (**1-PF$_6$**$\cdot 2CH_3CN$). Yield: 24 mg (17%). FAB-MS (NBA): $m/z$ 1041 ($[\mathbf{1}]^+$). Anal. Found (calcd for $C_{37}H_{48}N_5O_3F_6Mo_3PS_7$): C, 34.90 (35.05); H, 3.87 (3.82); N, 5.61 (5.52)%.

**Synthesis of $[Mo_3S_4(LSeMe)_3]PF_6 \cdot 1.5CH_3CN$ (2-PF$_6$$\cdot$ 1.5CH$_3$CN).** A sample of solid material containing the cation $[Mo_3S_4(H_2O)_9]^{4+}$ (0.11 mmol), which was obtained by removal of the solvent from a 5.61 mM solution of $[Mo_3S_4(H_2O)_9]^{4+}$ in hydrochloric acid (20.0 mL) was suspended in methanol (2 mL). A solution of HLSeMe (90 mg, 0.35 mmol) in methanol (10 mL) was added to the suspension, and the mixture was stirred for 12 h at room temperature. After the insoluble solid was removed by filtration, $NH_4PF_6$ (23 mg, 0.14 mmol) was added to the filtrate. Diethyl ether was then carefully layered on top of this solution and the mixture was allowed to stand to afford dark green crystals of $[Mo_3S_4(LSeMe)_3]PF_6 \cdot 1.5CH_3CN$ (**2-PF$_6$**$\cdot 1.5CH_3CN$). Yield: 30 mg (20%). FAB-MS (NBA): $m/z$ 1182 ($[\mathbf{2}]^+$). Anal. Found (calcd for $C_{36}H_{47}N_{4.5}O_3F_6Mo_3PS_4Se_3$): C, 31.12 (31.15); H, 3.57 (3.38); N, 4.38 (4.54)%. $^{77}$Se NMR ($CD_3CN$): $\delta$ 3.97.

**X-ray Crystallography.** A single-crystal X-ray structure determination was performed for complex **1-PF$_6$**. A single crystal was attached to Cryoloop using Paraton N. Diffraction data were collected at 123 K on a VariMax Saturn diffractometer with graphite-monochromated Mo K$\alpha$ radiation ($\lambda = 0.7107$ Å) using a rotation method. The data were integrated, scaled, sorted, and averaged using CrystalClear software.[11] Absorption corrections were applied using the multiscan method. The structures were solved using SHELX97,[12] expanded using Fourier techniques,[13] and refined by using full-matrix least-squares against $F^2$ with SHELXL97 equipped in the CrystalStructure 4.0.1 software.[14] All hydrogen atoms were located at the calculated positions and refined as riding models. Crystallographic data have been deposited with Cambridge Crystallographic Data Center: Deposition number CCDC-1023632.

## Results and Discussion

**Syntheses and Solid-State Structure of Complexes.** Schiff base ligands, obtained from the reactions of salicylaldehyde derivatives and a wide range of different amines, usually behave as multidentate ligands that provide very stable coordination environments, and most of their complexes adopt meridional fashion as previously reported.[15] On the other hand, Amosova et al. reported a different type of tridentate Schiff base ligands, synthesized using the condensation reactions of salicylaldehyde derivatives and functionalised alkyl amine derivatives (Chart 1).[16] In these Schiff base ligands, the length and flexibility of the alkyl chains that tether the third donor

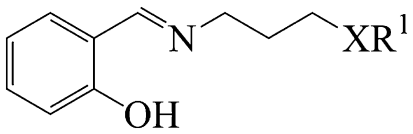


**Chart 1.** Fundamental framework of ligands (X = S, Se).

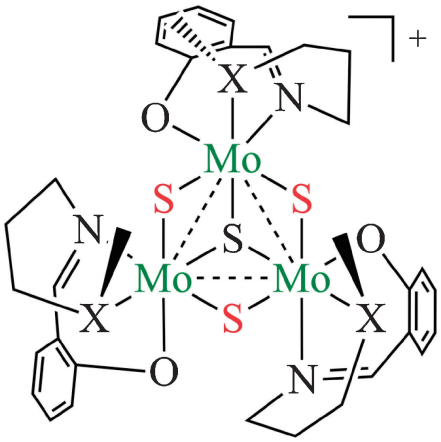


**Chart 2.** One of isomers of $\mathbf{1}^+$ (X = S) and $\mathbf{2}^+$ (X = Se).

atom to the Schiff base moiety are such that these tridentate ligands can adopt either meridional or facial coordination mode. Similar flexible Schiff base ligands coordinated in either meridional or facial fashion have been reported for multinuclear cubane Na(I) clusters and mono- and trinuclear Ni(II) complexes.[17] The ligands HLSMe and HLSeMe reported in this paper were prepared from the condensation reaction of salicylaldehyde and either 3-(methylthio)propylamine or 3-(methylseleno)propylamine. It was expected that the flexible propylene chains that connect the sulfur or selenium donor atoms in these tridentate ligands could facilitate coordination in either meridional or facial fashion.

The cationic complexes, $[Mo_3S_4(LXMe)_3]^+$ (X = S ($\mathbf{1}^+$), Se ($\mathbf{2}^+$)), were prepared from the reactions of $[Mo_3S_4(H_2O)_9]^{4+}$ and HLSMe or HLSeMe in methanol. The starting cationic material $[Mo_3S_4(H_2O)_9]^{4+}$ was prepared according to a previously reported procedure,[7] and stored in conc. hydrochloric acid. For the syntheses of $\mathbf{1}^+$ and $\mathbf{2}^+$, the hydrochloric acid solvent was first removed under reduced pressure to give a solid material that contained the cation $[Mo_3S_4(H_2O)_9]^{4+}$. This solid was then treated directly with the ligands HLSMe or HLSeMe to give **1-PF$_6$** or **2-PF$_6$**, respectively, after precipitation by the addition of $NH_4PF_6$. Removal of the excess acid before addition of HLSMe or HLSeMe was essential because acid suppresses the proton loss from the ligand that is required for tridentate coordination to the Mo centres and also greatly accelerates the rate of imine hydrolysis.

The solubility of the monocationic complexes $\mathbf{1}^+$ and $\mathbf{2}^+$ (Chart 2) depends on the counter anions. The chloride salts **1-Cl** and **2-Cl** are soluble in methanol but not in acetonitrile, while the $PF_6$ salts **1-PF$_6$** and **2-PF$_6$** are soluble in acetonitrile but not in methanol. All measurements of the complexes were performed using the $PF_6$ salts.

Crystallographic data and refinement details for complex **1-PF$_6$** are summarized in Table 1, and an ORTEP drawing of the complex cation (with the counter $[PF_6]^-$ anion omitted) is

**Table 1.** Crystallographic and Refinement Data for $[Mo_3S_4(LSMe)_3]$ (**1**)·$PF_6$·$2CH_3CN$

| | |
|---|---|
| Formula | $C_{37}H_{48}F_6Mo_3N_5O_3PS_7$ |
| Formula weight | 1268.02 |
| Crystal system | monoclinic |
| monoclinic | *Pn* (#7) |
| $a$/Å | 12.999(2) |
| $b$/Å | 11.240(2) |
| $c$/Å | 15.826(3) |
| $\beta$/degree | 91.501(3) |
| $V$/Å$^3$ | 2311.4(7) |
| Z | 2 |
| $D_{calcd}$/g cm$^{-3}$ | 1.822 |
| $\mu$ (Mo K$\alpha$)/cm$^{-1}$ | 12.180 |
| G.O.F. | 1.050 |
| $R_1$[a] ($I > 2.00\sigma(I)$) | 0.0331 |
| $R$; $wR_2$[b] | 0.0350; 0.0882 |

a) $R_1 = \sum ||F_o| - |F_c|| / \sum |F_o|$. b) $wR_2 = [\sum(w(F_o^2 - F_c^2)^2) / \sum w(F_o^2)^2]^{1/2}$.

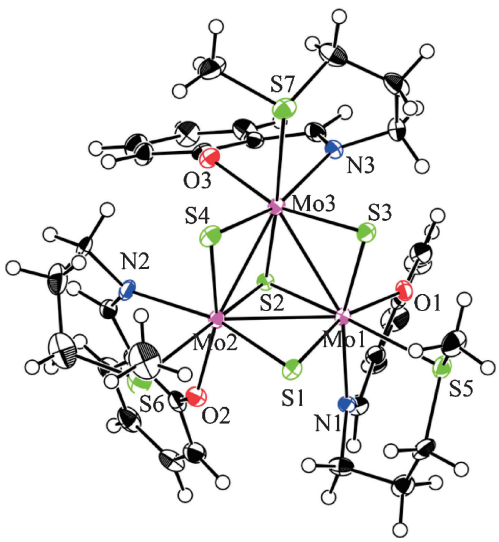


**Figure 1.** An ORTEP drawing of $[Mo_3S_4(LSMe)_3]$ (**1**)·$PF_6$·$2CH_3CN$. The counter anion of $PF_6$ and $CH_3CN$ molecules were omitted for clarity.

shown in Figure 1. The three Mo atoms and four bridging S atoms form an incomplete cubane-type core. Each Mo atom bonds to a LSMe ligand in a tridentate manner via the O, N, and S donor atoms. The S atoms of the three Schiff base ligands are located in the positions *trans* to the triply bridging sulfido ligand in the $Mo_3S_4$ core. The monocationic $Mo_3S_4$ cluster has the pseudo $C_3$ symmetry if the coordinated thioether moieties containing chiral S atoms are not taken into account. Because of the arrangements of the asymmetric Schiff base ligand, each molybdenum center possibly adopts one of two chiralities, which are designated by clockwise (*P*) or anticlockwise (*M*) as they relate to the rotation of the oxygen atoms around the $C_3$ axis with the capping sulfur pointing towards the viewer.[18] Furthermore, each sulfur atom of the three coordinated SMe groups in the complex cation is also chiral, which is defined as *R* or *S*. As a result, the two enantiomers, *P*-(*R*, *S*, *S*) and *M*-(*S*, *R*, *R*), were observed in the unit cell.

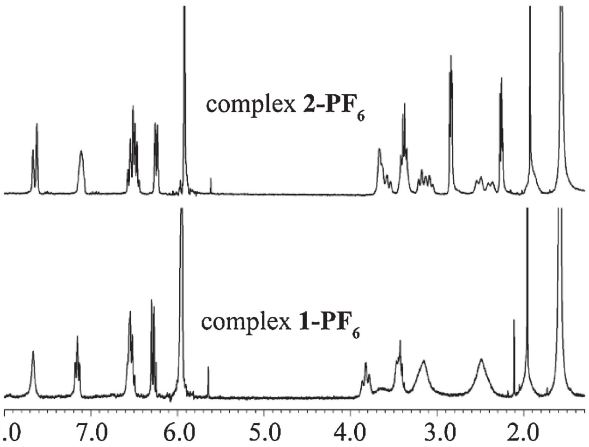


**Figure 2.** $^1$H NMR spectra of complexes **1-PF$_6$** and **2-PF$_6$** in $CDCl_2CDCl_2$ at room temperature.

The Mo–Mo distances (2.7719(6), 2.7519(7), and 2.7600(11) Å) are in the range of reported values (2.726(3)–2.8314(3) Å) for $Mo_3S_4$ incomplete cubane complexes.[19] No trends in the Mo–Mo distances depending on the properties of the different ancillary ligands such as donating ability are observed. The Mo–$\mu_3$-S and Mo–$\mu_2$-S distances, and the Mo–$\mu_3$-S–angles in the $Mo_3S_4$ core of **1-PF$_6$** are very similar to the corresponding distances and angles in the other previously reported $Mo_3S_4$ complexes (see Supporting Information Tables S1 and S2).

**Structures and Dynamic Behavior of the $Mo_3S_4$ Complexes in Solution.** The identities of complexes **1-PF$_6$** and **2-PF$_6$** in solution were confirmed by using FAB mass spectrometry, $^1$H (for **1-PF$_6$** and **2-PF$_6$**) and $^{77}$Se (for **2-PF$_6$**) NMR spectroscopy. In the FAB mass spectra of complexes **1-PF$_6$** and **2-PF$_6$**, peaks attributed to the cationic moieties **1**$^+$ and **2**$^+$ were observed at $m/z$ 1041 and 1182, respectively. $^{77}$Se NMR spectrum of complex **2-PF$_6$**, which contains the selenoether donor group, in $CD_3CN$ at room temperature exhibits one singlet signal at considerably higher magnetic field ($\delta$ 3.97) relative to the free HLSeMe ligand ($\delta$ 183.13) implying the differences in chemical shifts for the different configurational arrangements possible for the three selenium atoms are too small to detect.

$^1$H NMR spectra of **1-PF$_6$** and **2-PF$_6$** in deuterated 1,1,2,2-tetrachloroethane (Figure 2) did not exhibit two sets of signals for the LXMe ligands in each complex with a 1:2 ratio of their integrated intensities as expected by the result of the structural analysis of **1-PF$_6$** showing the pseudo $C_3$ symmetry of the monocationic complex with the *P*-(*R*, *S*, *S*)- or *M*-(*S*, *R*, *R*)-configuration. The signals for the SMe protons in **1-PF$_6$** appeared in the spectrum as two broad signals at room temperature. The broadening of the signals for the SMe protons suggested a flipping motion of the methyl group at the chiral sulfur center between the *R* and *S* configurations (Scheme 2). On the other hand, two sets of signals for the SeMe protons of **2-PF$_6$** were observed at room temperature.

To examine the details of the chiral inversion process, variable temperature (VT) $^1$H NMR spectroscopy was performed for both **1-PF$_6$** and **2-PF$_6$** (Figures 3 and 4). The SMe protons of **1-PF$_6$** were observed as two sets of triplet signals


 

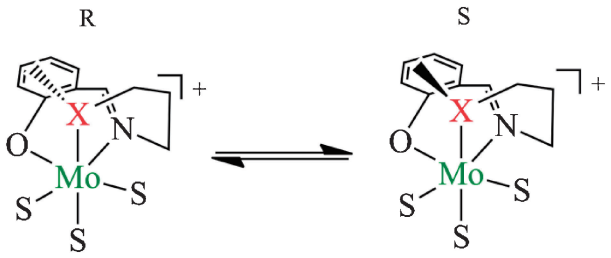


**Scheme 2.** Chiral inversion between *R* and *S* configurations at X atom (X = S, Se).

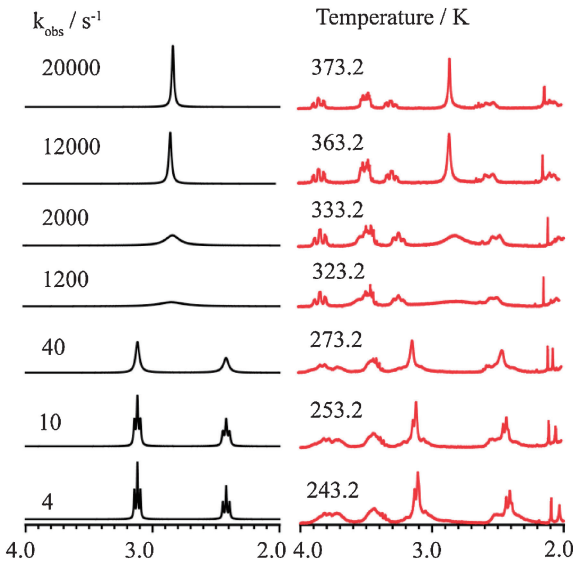


**Figure 3.** VT-$^1$H NMR spectra of the SMe region of **1-PF$_6$** (right) and the simulated spectra (left).

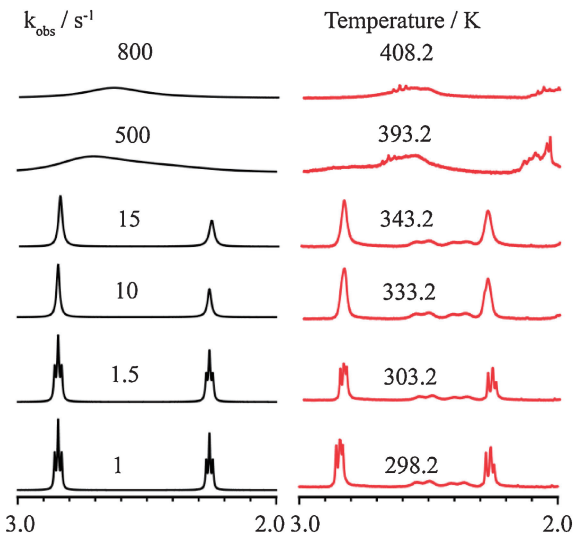


**Figure 4.** VT-$^1$H NMR spectra of the SeMe region of **2-PF$_6$** (right) and the simulated spectra (left).

coupled with the protons of the methylene adjacent to the S or Se atom at −30 °C and these signals merged into one sharp signal at 100 °C. In the case of **2-PF$_6$**, two sets of signals for the SeMe protons appeared at room temperature and the signals merged affording one broad signal even at 135 °C.

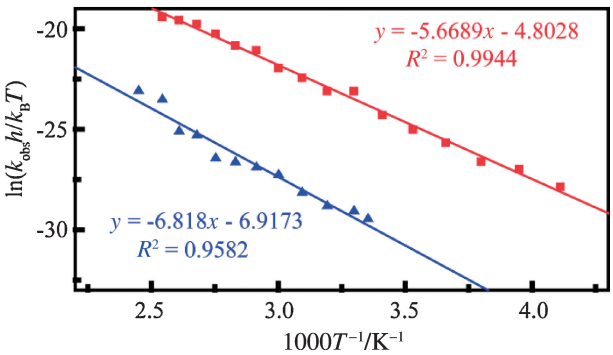


**Figure 5.** Eyring plots for **1-PF$_6$** (——) and **2-PF$_6$** (——) obtained from line shape analysis.

**Table 2.** Activation Parameters for S and Se Inversion in Complexes **1-PF$_6$** and **2-PF$_6$** in $CDCl_2CDCl_2$

| | $\Delta H^{\ddagger}$/kJ mol$^{-1}$ | $\Delta S^{\ddagger}$/J mol$^{-1}$ K$^{-1}$ |
|---|---|---|
| **1-PF$_6$** | 47.1 ± 0.9 | −39.9 ± 3.1 |
| **2-PF$_6$** | 56.7 ± 4.0 | −57.5 ± 11.8 |

Some of the isomers with a series of the combination of *S* and *R* configuration around the sulfur center, such as *P*-(*S*, *S*, *S*), *P*-(*R*, *S*, *S*), *P*-(*R*, *R*, *S*), *P*-(*R*, *R*, *R*), and their enantiomers, possibly exist in solution. Although these isomers possibly give some signals of the SMe or SeMe protons, only two signals for the SMe or SeMe protons with a 0.7:1 ratio were observed. This result suggests that there are only small influences by the adjacent Schiff base ligands and the chemical shifts of the XMe protons are scarcely affected by the neighboring LXMe ligands. In other words, all XMe groups were located in similar environments in the $Mo_3S_4$ core, and the chemical shifts of the XMe protons depend only on the *R* and *S* configurations at the chalcogenide centers. In addition, the other signals for the LXMe ligands except for the signals of the imine protons in the complexes were indistinguishable even at low temperatures (described above). These observations revealed that these cationic clusters maintain the pseudo $C_3$ symmetry in solution and the dynamic behavior of the inversion process can be simplified as the inversion between *P*-*R* and *P*-*S* or *M*-*S* and *M*-*R*, respectively (Scheme 2).

Line shape analyses were applied to the VT-NMR data to obtain rate constants of these inversion processes for each complex (Figures 3 and 4). The Eyring plots using the rate constants for each temperature are presented in Figure 5 providing the activation parameters, $\Delta S^{\ddagger}$ and $\Delta H^{\ddagger}$, listed in Table 2. The $\Delta H^{\ddagger}$ value for **2-PF$_6$** is larger than that for **1-PF$_6$** reflecting the stronger Mo–Se bond in **2-PF$_6$** than the Mo–S bond in **1-PF$_6$**. In general, s character of the lone pairs on chalcogen atoms increases for heavier elements, thus the lone pair on a Se atom has more s character than S,[20] which affects σ-donating ability of the ligands containing Se and S donating atoms resulting in the stronger Mo–Se bond for **2-PF$_6$**. Both the $\Delta S^{\ddagger}$ values for **1-PF$_6$** and **2-PF$_6$** are negative implying that the chiral inversion at the S or Se atom involves aggregation processes of the complexes and solvent molecules. These results suggest that the inversion processes proceed via Mo–S or Mo–Se bond cleavage accompanied by the coordination of the solvent molecules.

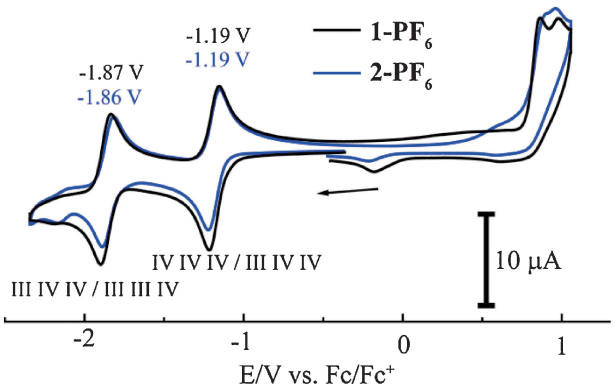


**Figure 6.** Cyclic voltammograms of **1-PF$_6$** (0.5 mM) and **2-PF$_6$** (0.5 mM) in $CH_3CN$ containing 0.1 M *n*-$Bu_4NPF_6$ (scan rate: 100 mV $s^{-1}$).

There might be a possibility of the existence of the other complex dynamic processes involving the adjacent coordination sites in solution because the Mo–S and Mo–Se bonds in the trans position to the triply-bridging S atom in the complexes are less labile than the others as reported. Stabilization by the chelate effect of the coordination of the salicylaldimine probably overcomes this disadvantage.

**Electrochemical Properties of Complexes of 1-PF$_6$ and 2-PF$_6$.** The electrochemical properties of complexes **1-PF$_6$** and **2-PF$_6$** were examined using cyclic voltammetry in acetonitrile and the results are shown in Figure 6. Complexes **1-PF$_6$** and **2-PF$_6$** gave similar cyclic voltammograms (Figure 6) and each complex exhibited two consecutive reversible one-electron reduction waves at −1.2 and −1.9 V, clearly showing that the thioether and selenoether moieties in **1-PF$_6$** and **2-PF$_6$** afford no significant influence on the reduction potentials. The fact that the two one-electron reductions proceeded stepwise suggests the existence of electronic communication among the Mo centers. Results of DFT calculations (vide infra) imply that the reductions occurred at the $Mo_3(\mu_2\text{-}S)_3$ moiety. Therefore, it is probably better to use the combined formal oxidation states of the three metal ions in the $Mo_3S_4$ units (i.e. XII, XI, and X in the monocationic, neutral, and monoanionic complexes, respectively) rather than the hypothetical individual metal oxidation states (IV IV IV), (III IV IV), and (III III IV), which are presented in Figure 6 for clarity.

To investigate the potential catalytic ability of the $Mo_3S_4$ complexes in a proton reduction reaction, cyclic voltammometry experiments were carried out for complexes **1-PF$_6$** and **2-PF$_6$** in the presence of 1, 2, 3, 10, 20, 30, and 40 equiv. of $CH_3CO_2H$ as a proton source (Figures 7 and 8). The results of the VT $^1$H NMR measurements revealed that the sulfur or selenium atoms in the flexible arms of the propyl chains dissociate from the metal centers in solution providing the vacant site on the metal centers. These results also implied that the free sulfur and selenium atoms dissociated from the metal center possibly work as a proton relay for the proton reduction reaction, however no differences in the reactivity with proton between **1-PF$_6$** and **2-PF$_6$** were observed suggesting the sulfur and selenium atoms do not perform such roles. Catalytic currents were observed around the potentials of the second reduction for **1-PF$_6$** and **2-PF$_6$**, and the overpotentials for the

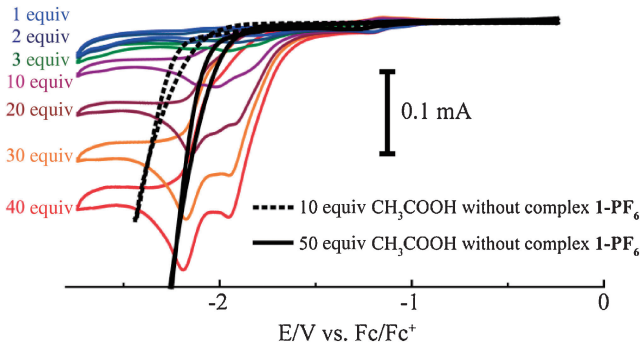


**Figure 7.** Cyclic voltammograms of **1-PF$_6$** recorded with variable equivalents of $CH_3COOH$.

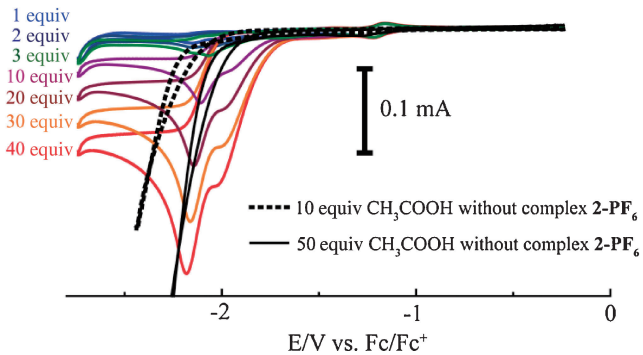


**Figure 8.** Cyclic voltammograms of **2-PF$_6$** recorded with variable equivalents of $CH_3COOH$.

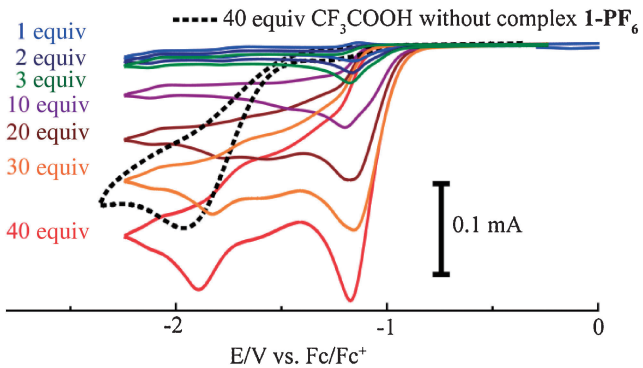


**Figure 9.** Cyclic voltammograms of complex **1-PF$_6$** recorded with variable equivalents of $CF_3COOH$.

proton reductions catalized by **1-PF$_6$** or **2-PF$_6$** were smaller than those for the heterogeneous proton reduction of $CH_3CO_2H$ in the absence of **1-PF$_6$** or **2-PF$_6$**. On the other hand, the cyclic voltammogram of **1-PF$_6$** in the presence of $CF_3CO_2H$ as a proton source showed catalytic current around the potentials of the first reduction (Figure 9). These results can be explained if the p$K_a$ of the protonated form of **1**$^+$ lies between the p$K_a$'s of $CF_3CO_2H$ and $CH_3CO_2H$, and protonation of the complex therefore occurred in the presence of the stronger acid, $CF_3CO_2H$ before reduction. As a consequence, a CECE process is observed, while an ECEC process is dominant in the presence of a weaker acid, $CH_3CO_2H$.

DFT calculations of complex **1**$^+$ and its one and two electron-reduced species were performed to rationalize the observed reactivity of these species with $H^+$ in the CV measurements.[21]


 

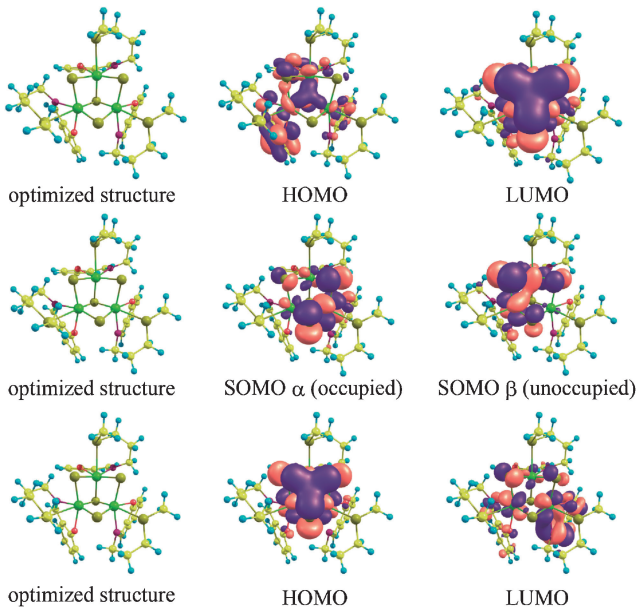


**Figure 10.** MOs of the isolated monocationic species (top) and the one (middle) or two (bottom) electron reduced species of complex $\mathbf{1}^{+}$.

Optimized structures (Figure 10) were obtained using the B3LYP density functional method with the LanL2DZ basis set for Mo and the 6-31g** basis set for the others. The optimized structure of $\mathbf{1}^{+}$ is well reproduced in the X-ray structure. There are no significant differences among the optimized structures of complex $\mathbf{1}^{+}$ and its one and two electron-reduced species. These structural features of the complexes are consistent with the reversibility of the reduction waves observed in the CV measurement of complex **1-PF$_6$** suggesting small structural changes upon the reductions. The energy levels of HOMO and LUMO and their gaps for complexes $\mathbf{1}^{+}$ and $\mathbf{2}^{+}$ (See Table S7 in the Supporting Information) are similar to each other, despite having different donating atoms of S or Se in the flexible arms. These results are consistent with the similar redox potentials of **1-PF$_6$** and **2-PF$_6$**. On the other hand, no contribution of the S and Se atoms in the flexible arms to the HOMO and LUMO was found. The bonding orbitals of the coordination bonds of the S and Se atoms in the flexible arms toward the molybdenum centers appeared as HOMO−10 at −9.1673 eV and HOMO−9 at −9.0168 eV, respectively. This difference may be attributed to the donating abilities of the S and Se atoms and probably contributes to the cleavages of the Mo–S and Mo–Se bonds observed in the VT-NMR measurements. For $\mathbf{1}^{+}$, the HOMO components are distributed over the phenyl rings of the Schiff base ligands and the $Mo_3S_4$ cluster core, and for the LUMO large orbital contributions are found from the $Mo_3S_4$ core, especially the doubly bridging sulfido ligands. This implies that in the reduction of $\mathbf{1}^{+}$ the first electron adds primarily to the $Mo_3(\mu_2\text{-}S)_3$ moiety. For the 1 electron-reduced species, the SOMO components for the α and β spins are localized on the $Mo_3(\mu_2\text{-}S)_3$ moiety and the sum of the SOMOs is similar to the LUMO of $\mathbf{1}^{+}$. The HOMO of the 2 electron-reduced species is also very similar to the LUMO of $\mathbf{1}^{+}$.

As previously reported, the doubly bridging sulfido ligands in the $Mo_3S_4$ core react with various metals affording mixed-metal cubane-type sulfide clusters.[19c] These facts show the nucleophilicity of the doubly bridging sulfido ligands. In our case, while the nucleophilicity of the doubly bridging sulfido ligands is not basic enough to capture protons before the reduction of the complex, the nucleophilicity is probably increased after the reduction resulting in the protonation at the doubly bridging sulfido ligands.

## Conclusion

We have introduced the two kinds of Schiff base ligands, HLXMe (X = S or Se) into $Mo_3S_4$ complexes as a fundamental framework for the tuning of electrochemical properties of the complexes. X-ray structural analysis of thioether complex **1-PF$_6$** showed pseudo $C_3$ symmetry for the complex and *P*-(*R*, *S*, *S*)- or *M*-(*S*, *R*, *R*)-configurations around the sulfur atoms of the thioether moieties in the complex. Variable temperature $^1$H NMR spectroscopy of complexes **1-PF$_6$** and **2-PF$_6$** revealed that the *R* and *S* configurations are under equilibrium in solution and the kinetic constants of **1-PF$_6$** are larger than those of **2-PF$_6$** at each temperature due to the weaker σ donating ability for the coordinated sulfur atoms of the thioether moieties than that of the selenium atoms of the selenoether. Cyclic voltammetry exhibited two consecutive reversible one-electron reduction waves for each complex and showed catalytic current in the presence of a proton source. The reduction potentials for the catalytic waves depended on the acidity of acids used as proton sources. DFT calculations of the complexes suggested that the protonation reaction should occur at the doubly bridging sulfido ligands. These experimental and theoretical results will supply some information about the roles of the doubly bridging sulfur ligands of the $Mo_3S_4$ core on the catalytic proton reduction.

We thank Professor Takashi Shibahara of Okayama University of Science for valuable suggestions regarding the preparation of $[Mo_3S_4(H_2O)_9]^{4+}$. We also thank Professor L. James Wright of University of Auckland for helpful discussions.

## Supporting Information

NMR spectra, Detail of crystallographic analysis of **1**, and DFT calculations. This material is available electronically on J-STAGE.

## References

1 R. M. Navarro, M. A. Peña, J. L. G. Fierro, *Chem. Rev.* **2007**, *107*, 3952.

2 R. H. Crabtree, *Energy Production and Storage: Inorganic Chemistry Strategies for Warning World*, John Wiley & Sons Inc., New York, **2010**.

3 a) K. Sakai, K. Matsumoto, *J. Coord. Chem.* **1988**, *18*, 169. b) K. Sakai, K. Matsumoto, *J. Mol. Catal.* **1990**, *62*, 1. c) K. Sakai, Y. Kizaki, T. Tsubomura, K. Matsumoto, *J. Mol. Catal.* **1993**, *79*, 141. d) K. Sakai, H. Ozawa, *Coord. Chem. Rev.* **2007**, *251*, 2753.

4 a) H. I. Karunadasa, E. Montalvo, Y. Sun, M. Majda, J. R. Long, C. J. Chang, *Science* **2012**, *335*, 698. b) J. Kibsgaard, T. F. Jaramillo, F. Besenbacher, *Nat. Chem.* **2014**, *6*, 248.

5 T. Shibahara, *Coord. Chem. Rev.* **1993**, *123*, 73.

6 R. Hernandez-Molina, M. N. Sokolov, A. G. Sykes, *Acc. Chem. Res.* **2001**, *34*, 223.

7 T. Shibahara, M. Yamasaki, G. Sakane, K. Minami, T. Yabuki, A. Ichimura, *Inorg. Chem.* **1992**, *31*, 640.
8 Y. Hou, B. L. Abrams, P. C. K. Vesborg, M. E. Björketun, K. Herbst, L. Bech, A. M. Setti, C. D. Damsgaard, T. Pedersen, O. Hansen, J. Rossmeisl, S. Dahl, J. K. Nørskov, I. Chorkendorff, *Nat. Mater.* **2011**, *10*, 434.
9 S. W. Seo, S. Park, H.-Y. Jeong, S. H. Kim, U. Sim, C. W. Lee, K. T. Nam, K. S. Hong, *Chem. Commun.* **2012**, *48*, 10452.
10 For example: a) M. E. Carroll, B. E. Barton, T. B. Rauchfuss, P. J. Carroll, *J. Am. Chem. Soc.* **2012**, *134*, 18843. b) M. P. Stewart, M.-H. Ho, S. Wiese, M. L. Lindstrom, C. E. Thogerson, S. Raugei, R. M. Bullock, M. L. Helm, *J. Am. Chem. Soc.* **2013**, *135*, 6033. c) Z. Han, L. Shen, W. W. Brennessel, P. L. Holland, R. Eisenberg, *J. Am. Chem. Soc.* **2013**, *135*, 14659.
11 *CrystalClear: Software Package*, Rigaku Corporation, **1999**.
12 G. M. Sheldrick, *SHELXS-97, Program for Crystal Structure Refinement*, University of Göttingen, Germany, **1997**.
13 P. T. Beurskens, G. Admiraal, G. Beurskens, W. Bosman, P. R. de Gelder, R. Israel, J. M. M. Smits, *The DIRDIF-99 Program System*, Technical Report of the Crystallography Laboratory, University of Nijmegen, The Netherlands, **1999**.
14 *Crystal Structure Analysis Package*, Rigaku and Rigaku/MSC, TX, USA, **2000–2006**.
15 a) K. Takano, M. Takahashi, T. Fukushima, M. Takezaki, T. Tominaga, H. Akashi, H. Takagi, T. Shibahara, *Bull. Chem. Soc. Jpn.* **2012**, *85*, 1210. b) K. Kawamoto, H. Akashi, M. Yamasaki, T. Shibahara, *Chem. Lett.* **2013**, *42*, 389.
16 S. V. Amosova, N. A. Makhaeva, A. V. Martynov, V. A. Potapov, B. R. Steele, I. D. Kostas, *Synthesis* **2005**, 1641.
17 X. Song, Z. Wang, J. Zhao, T. S. A. Hor, *Chem. Commun.* **2013**, *49*, 4992.
18 a) M. Feliz, E. Guillamón, R. Llusar, C. Vicent, S.-E. Stiriba, J. Pérez-Prieto, M. Barberis, *Chem.—Eur. J.* **2006**, *12*, 1486. b) R. Frantz, E. Guillamón, J. Lacour, R. Llusar, V. Polo, C. Vicent, *Inorg. Chem.* **2007**, *46*, 10717. c) A. G. Algarra, M. G. Basallote, M. J. Fernández-Trujillo, M. Feliz, E. Guillamón, R. Llusar, I. Sorribes, C. Vicent, *Inorg. Chem.* **2010**, *49*, 5935.
19 a) T. Yamauchi, H. Takagi, T. Shibahara, H. Akashi, *Inorg. Chem.* **2006**, *45*, 5429. b) T. Shibahara, H. Kuroya, *Polyhedron* **1986**, *5*, 357. c) R. Yoshida, T. Shibahara, H. Akashi, *Bull. Chem. Soc. Jpn.* **2013**, *86*, 839. d) I. Takei, K. Suzuki, Y. Enta, K. Dohki, T. Suzuki, Y. Mizobe, M. Hidai, *Organometallics* **2003**, *22*, 1790. e) H. Akashi, T. Shibahara, H. Kuroya, *Polyhedron* **1990**, *9*, 1671. f) M. Yamasaki, T. Shibahara, *Anal. Sci.* **1992**, *8*, 727.
20 E. W. Abel, A. R. Khan, K. Kite, K. G. Orrell, V. Šik, J. C. S. Dalton, *J. Chem. Soc., Dalton Trans.* **1980**, 1175.
21 M. J. Frisch, G. W. Trucks, H. B. Schlegel, G. E. Scuseria, M. A. Robb, J. R. Cheeseman, G. Scalmani, V. Barone, B. Mennucci, G. A. Petersson, H. Nakatsuji, M. Caricato, X. Li, H. P. Hratchian, A. F. Izmaylov, J. Bloino, G. Zheng, J. L. Sonnenberg, M. Hada, M. Ehara, K. Toyota, R. Fukuda, J. Hasegawa, M. Ishida, T. Nakajima, Y. Honda, O. Kitao, H. Nakai, T. Vreven, J. A. Montgomery, Jr., J. E. Peralta, F. Ogliaro, M. Bearpark, J. J. Heyd, E. Brothers, K. N. Kudin, V. N. Staroverov, R. Kobayashi, J. Normand, K. Raghavachari, A. Rendell, J. C. Burant, S. S. Iyengar, J. Tomasi, M. Cossi, N. Rega, J. M. Millam, M. Klene, J. E. Knox, J. B. Cross, V. Bakken, C. Adamo, J. Jaramillo, R. Gomperts, R. E. Stratmann, O. Yazyev, A. J. Austin, R. Cammi, C. Pomelli, J. W. Ochterski, R. L. Martin, K. Morokuma, V. G. Zakrzewski, G. A. Voth, P. Salvador, J. J. Dannenberg, S. Dapprich, A. D. Daniels, Ö. Farkas, J. B. Foresman, J. V. Ortiz, J. Cioslowski, D. J. Fox, *Gaussian 09 (Revision D.01)*, Gaussian, Inc., Wallingford CT, **2009**.


 